

Numerical Continuation of Solutions and Bifurcation Analysis in Multibody Systems Applied to Motorcycle Dynamics

J. P. MEIJAARD* and A. A. POPOV

*School of Mechanical, Materials and Manufacturing Engineering, University of Nottingham, University Park, Nottingham NG7 2RD, U.K.; *Author for correspondence (e-mail: jaap.meijaard@nottingham.ac.uk; fax: +44-115-9513800)*

(Received: 3 February 2004; accepted: 22 September 2004)

Abstract. It is shown how the equations of motion for a multibody system can be generated in a symbolic form and the resulting equations can be used in a program for the analysis of nonlinear dynamical systems. Stationary and periodic solutions are continued when a parameter is allowed to vary and bifurcations are found. The variational or linearized equations and derivatives with respect to parameters are also provided to the analysis program, which enhances the efficiency and accuracy of the calculations.

The analysis procedure is firstly applied to a rotating orthogonal double pendulum, which serves as a test for the correctness of the implementation and the viability of the approach. Then, the procedure is used for the analysis of the dynamics of a motorcycle. For running straight ahead, the nominal solution undergoes Hopf bifurcations if the forward velocity is varied, which lead to periodic wobble and weave motions. For stationary cornering, wobble instabilities are found at much lower speeds, while the maximal speed is limited by the saturation of the tyre forces.

Key words: bifurcations, continuation, double pendulum, motorcycle dynamics, multibody dynamics

1. Introduction

Several formalisms for deriving the equations of motion for multibody systems, which are mechanical systems consisting of interconnected and interacting bodies, have been developed and coded in computer programs that are widely available. A partial overview of these multibody system dynamics formalisms and programs can be found in edited volumes [1, 2] and review articles [3, 4]. Some of these programs yield explicit symbolic expressions for the equations of motion, while others deliver the accelerations in a numeric form for set values of the system parameters and state variables. For both program types, the analysis of a system consists mainly in repeated simulations of the motion with given parameter values and initial conditions. For some programs it is also possible to determine the linearized equations about some working point and the sensitivities with respect to parameter variations.

Besides these transient solutions, one is often interested in the general structure of possible solutions for a set of different initial conditions. In particular, the ultimate behaviour of solutions, after all phenomena caused by the special choice of the initial conditions have faded away, is often required. If the transients decay slowly, as it can be in lightly damped systems, the simulations may take a long time and methods for calculating the limit behaviour directly are more efficient. Furthermore, it is often desirable to know some unstable stationary or periodic solutions, for instance to obtain an estimate for the size of the basin of attraction of stable solutions, which cannot easily be found by simulation. Numerical methods for a direct calculation of the two simplest types of limit behaviour, stationary and periodic solutions, are available, and these methods can also determine the stability of these types of solutions by means of a linearization of the equations at a solution.

In addition, it is of interest to know how the limit solutions develop as parameters are varied. With the aid of numerical path-following or continuation methods, branches of stationary and periodic solutions can be computed if a system parameter is varied. Local bifurcations are detected by examining changes in the stability of the solution along the branch. A survey of methods and available programs is given in [5]. An overview of bifurcations for stationary and periodic solutions can be found in textbooks such as [6–8].

Programs for the dynamics of multibody systems and programs for numerical continuation of solutions and bifurcation analysis are widely available now, but little attention has been paid to the application of the latter to the equations generated by the former. Continuation methods have been applied to kinematic design problems [9, 10], where the equations are explicitly given and the solution procedure makes use of the special structure of these equations. An extensive body of literature deals with the continuation of parameter-dependent static solutions for large finite-element models and the determination of their bifurcation points [11]. Some of these methods are available in most nonlinear general-purpose finite element codes. The direct determination of bifurcation points is discussed in [12]. In [13], a continuation method was used to find branches of static solutions for multibody systems. Meijaard [14, 15] initiated the application to finding branches of periodic solutions for rigid as well as flexible multibody systems.

In this article it is first shown how the equations of motion generated by a symbolic multibody program can be used directly in a freely available continuation program to calculate branches of stationary and periodic solutions together with bifurcations of these solutions. Then, an application to a simple problem, a rotating orthogonal double pendulum, is considered, in order to test the correctness of the implementation and the viability of the approach. Finally, the dynamic behaviour of a motorcycle is investigated. The cases of running straight ahead and stationary cornering are considered. In both cases, the stationary solution, with the speed as a variable parameter, can undergo Hopf bifurcations and the resulting periodic solutions are analysed.

2. Analysis Methods

2.1. SYMBOLIC MULTIBODY PROGRAM

In the presented approach, the equations of motion are generated in a symbolic form by the multibody dynamics program AutoSim [16–19]. This program can handle systems of rigid bodies that are interconnected by prismatic, revolute, and spherical joints or combinations of these and are arranged in a tree, which means that the graph of connections has a tree structure. Additional holonomic and nonholonomic constraints can be added for modelling special joints or closed kinematic loops, where the graph of connections has circuits. For the additional holonomic constraints, the dependent coordinates cannot generally be expressed explicitly in terms of the independent coordinates by elementary functions; this requires a numerical solution and destroys the purely symbolic character of the equations. Nonholonomic constraints are linear in the velocities for all practical applications, so these can be solved explicitly for the dependent velocities.

The methods used in AutoSim for deriving the equations of motion are mainly based on Kane's approach [20], with some modifications. The program is written in the interactive programming language Lisp [21] and consists of a set of definitions for functions, macros, and data structures. The definitions yield procedures for handling symbolic expressions, for modelling components of multibody systems such as rigid bodies, joints, constraints and forces, for adding user-defined equations, for deriving the

equations of motion, and for generating output. Although the input can be entered interactively, it is usually prepared in an input file consisting of a series of Lisp forms. All standard facilities of Lisp remain available, which makes it possible to extend the program with user-defined functions.

Here, the output consists of a main program written in Fortran-77, the same language as used by the continuation program. This main program contains a subroutine that returns the right-hand sides of the differential equations for given values of the time, state, and parameters, as well as subroutines for initialization, reading system and simulation parameters, numerical integration, and generating output.

For systems of bodies in a tree arrangement, the generated equations of motion have the form

$$\begin{aligned}\dot{\mathbf{q}} &= \mathbf{S}(\mathbf{q})\mathbf{u}, \\ \dot{\mathbf{u}} &= \mathbf{M}(\mathbf{q})^{-1}\mathbf{Q}(t, \mathbf{q}, \mathbf{u}, \mathbf{z}), \\ \dot{\mathbf{z}} &= \mathbf{g}(t, \mathbf{q}, \mathbf{u}, \mathbf{z}).\end{aligned}\tag{1}$$

Here, a dot over a variable denotes a total derivative with respect to the time t , and the state variables are the generalized coordinates, \mathbf{q} , the generalized velocities, \mathbf{u} , and the additional user-defined state variables, \mathbf{z} . The matrix \mathbf{S} , depending on the generalized coordinates, relates the rates of the generalized coordinates to the generalized velocities. In many cases, this is an identity matrix. \mathbf{M} is the system mass matrix and all forces and gyroscopic inertia terms are collected in the vector \mathbf{Q} . The rates of the additional state variables are given by the user-defined vector function \mathbf{g} .

2.2. CONTINUATION AND BIFURCATION ANALYSIS

For the analysis of solutions for the equations of motion, the numerical continuation program AUTO [22–24] is used. This program can perform a limited bifurcation analysis of systems of autonomous first-order differential equations depending on parameters as

$$\dot{\mathbf{x}} = \mathbf{f}(\mathbf{x}, \boldsymbol{\lambda}),\tag{2}$$

where \mathbf{x} is the vector of state variables and the vector $\boldsymbol{\lambda}$ contains the system parameters. In particular, it can analyse stationary and periodic solutions. Stationary solutions are characterized by the vanishing of the right-hand sides of Equation (2). On the other hand, periodic solutions are first discretized by a piecewise approximation with polynomials, which are subsequently required to satisfy the differential equations at discrete collocation points. The numeric periodic solutions are the zeros of the resulting equations. In order to make the solution unique for the autonomous systems, an integral phase condition is used.

If one parameter is made to vary, branches of these solutions can be determined by the familiar pseudo-arclength method [5]. Although the derivatives can be approximated by finite differences, more stable and accurate results are obtained, and even some efficiency is gained for most but the smallest systems, if the Jacobian matrix and parameter sensitivities,

$$\mathbf{J}(\mathbf{x}, \boldsymbol{\lambda}) = \frac{\partial \mathbf{f}(\mathbf{x}, \boldsymbol{\lambda})}{\partial \mathbf{x}} \quad \text{and} \quad \frac{\partial \mathbf{f}(\mathbf{x}, \boldsymbol{\lambda})}{\partial \boldsymbol{\lambda}},\tag{3}$$

are explicitly supplied to the continuation method. The stability of stationary solutions can be investigated by calculating the eigenvalues of the Jacobian matrix, while the stability of periodic solutions is determined by the characteristic multipliers, that is, the eigenvalues of the monodromy matrix [6].

Along the solution branch, local bifurcations characterized by the eigenvalues of the Jacobian matrix or monodromy matrix are detected. With two variable parameters, branches of bifurcation points can also be determined. For stationary solutions, branches of Hopf bifurcations and of saddle-node bifurcations can be calculated, whereas for periodic solutions, branches of saddle-node bifurcations and period-doubling bifurcations can be calculated.

2.3. COUPLING OF PROGRAMS FOR MULTIBODY DYNAMICS AND CONTINUATION OF SOLUTIONS

As already mentioned, it is advantageous for coupling the continuation program with the multibody dynamics code to have the disposal of the Jacobian matrix and the derivatives with respect to parameters as given in Equation (3). With the extensibility of the program, it was possible to write a procedure for generating linearized (or variational) equations and derivatives with respect to parameters. A standard option for linearizing is available, but this did not suit present needs: it was not possible to generate Fortran output and there was less control on the choice of variables and parameters. With the available formula manipulation function for partial differentiation this extension could be obtained relatively easily.

In the arguments of the function that computes these derivatives, the user can specify the state variables and parameters with respect to which the derivatives have to be extracted. For the determination of stationary and periodic solutions, it is necessary to exclude some cyclic coordinates, because these may contain secular terms, that is, they may be given by the sum of a linearly varying and a periodic function. This exclusion is allowed, because these coordinates do not appear explicitly in the equations of motion. The examples given below illuminate this aspect. The linearized equations are added to the system of differential equations as in Equation (1) for the user-defined state variables \mathbf{z} . Since the numbering convention for the continuation methods differs from that of the multibody dynamics software, an interfacing subroutine is needed to handle this book-keeping.

3. Rotating Orthogonal Double Pendulum

In a first example, the motion of a rotating double pendulum is analysed. For this simple problem, all equations can be derived with pencil and paper, and the equations obtained by the program can be directly checked as a validation for the procedures. This example contains the main ingredients of more complicated examples, such as a cyclic coordinate and user-defined state variables. As a main application, the dynamics of a motorcycle running in a straight line on a level road or negotiating a curve with constant radius are analysed in the next section.

The configuration of the rotating orthogonal double pendulum is shown in Figure 1. A similar system has been considered in [25, 26], where, however, no use was made of numerical continuation and bifurcation analysis procedures. The present example differs from those in [25, 26] in the mass distribution, the orthogonal arrangement of the hinges, and the damping model. The considered model has some practical applications: firstly, it can be seen as a crude model for the motion of a rolling aircraft [27]; secondly, it can be used to model one of the possible configurations for a centrifuge with static self-balancing.

The double pendulum is built up from two massless rigid rods with length ratio λ , three hinges, and a bob that has its mass m concentrated in a point. The base of the first hinge is connected to the earth, considered as an inertial system, and this hinge acts as a swivel with vertical axis. The second hinge is between the trunnion of the swivel and the first rod, the upper arm of length λl , and has its axis in

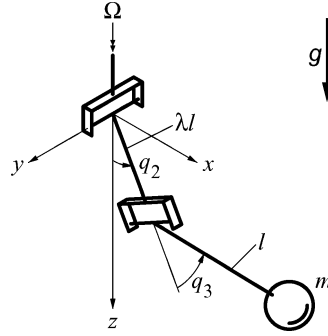


Figure 1. Configuration of the double pendulum.

a horizontal plane and perpendicular to the longitudinal axis of the upper arm. The other end of the upper arm is connected to the second rod, the lower arm of length l , by the third hinge, whose axis is perpendicular to the axis of the second hinge and the longitudinal axes of both rods. The bob is rigidly attached to the other end of the lower arm. The system is subjected to a uniform gravitational field of strength g in the downward direction.

The configuration of the system is described by the three rotation angles of the hinges, q_1 , q_2 , and q_3 , measured from the vertically down-hanging position, as indicated in Figure 1. The rotation angle of the swivel, q_1 , is clearly a cyclic coordinate. The angular velocity of the first hinge is prescribed, $\dot{q}_1 = \Omega(t)$, which imposes an integrable nonholonomic constraint, which is sometimes called a semiholonomic constraint [28]. A viscous isotropic external damping with damping coefficient c_e acts on the bob; that is, the damping force is $-c_e \mathbf{v}$ if \mathbf{v} is the velocity of the bob. The second and third hinges have an internal damping of the Maxwell type, represented by a dashpot and a spring in series. The distortion of the spring is chosen as an internal state variable. With the spring stiffness k_2 , the damping coefficient c_2 , and the distortion of the spring q_{k2} , the restoring moment in the second hinge is given by

$$M_2 = k_2 q_{k2} = c_2 (\dot{q}_2 - \dot{q}_{k2}). \quad (4)$$

This yields the differential equation for the internal state variable as

$$\dot{q}_{k2} = -(k_2/c_2) q_{k2} + \dot{q}_2. \quad (5)$$

Similarly, one has for the third hinge

$$\dot{q}_{k3} = -(k_3/c_3) q_{k3} + \dot{q}_3. \quad (6)$$

A system of first-order differential equations that describes the motion can be derived as

$$\begin{aligned} \dot{q}_1 &= \Omega, \\ \dot{q}_2 &= u_1, \\ \dot{q}_3 &= u_2, \\ \dot{u}_1 &= -\{\dot{\Omega} \cos q_2 \sin q_3 - \Omega^2 (\lambda + \cos q_3) \sin q_2 \cos q_2 + 2\Omega u_2 \cos q_2 \cos q_3 \\ &\quad - 2u_1 u_2 \sin q_3 + (g/l) \sin q_2 + k_2 q_{k2} / [ml^2 (\lambda + \cos q_3)] \\ &\quad + (c_e/m) [\Omega \cos q_2 \sin q_3 + u_1 (\lambda + \cos q_3)]\} / (\lambda + \cos q_3), \end{aligned}$$

$$\begin{aligned}
\dot{u}_2 = & -\{-\dot{\Omega}(1 + \lambda \cos q_3) \sin q_2 + \Omega^2(\lambda \sin^2 q_2 - \cos^2 q_2 \cos q_3) \sin q_3 \\
& - 2\Omega u_1(\lambda + \cos q_3) \cos q_2 \cos q_3 + u_1^2(\lambda + \cos q_3) \sin q_3 \\
& + (g/l) \cos q_2 \sin q_3 + k_3 q_{k3}/(ml^2) \\
& + (c_e/m)[- \Omega(1 + \lambda \cos q_3) \sin q_2 + u_2]\}, \\
\dot{q}_{k2} = & -(k_2/c_2)q_{k2} + u_1, \\
\dot{q}_{k3} = & -(k_3/c_3)q_{k3} + u_2.
\end{aligned} \tag{7}$$

Here, the first equation identifies the time derivative of the rotation angle of the first hinge with the prescribed angular velocity, which can directly be integrated, and the second and third equations give the definition of the angular velocities u_1 and u_2 of the second and third hinge. The vector of state variables is given by $\mathbf{x}^T = (\mathbf{q}^T; \mathbf{u}^T; \mathbf{z}^T) = (q_1, q_2, q_3; u_1, u_2; q_{k2}, q_{k3})$.

Only results for the case of a constant angular velocity Ω will be given; in this case Ω becomes a system parameter and q_1 increases linearly with time. Further results, also for harmonically varying angular velocities, can be found in [29]. For the numerical investigations, the parameter values $m = 1$, $l = 1$, $g = 1$, $\lambda = 0.2$, $c_2 = 0.01$, $c_3 = 0.01$, $k_2 = 0.1$, and $k_3 = 0.1$ are chosen. This means that the equations are made dimensionless with the parameters m , l , and g , the lower arm is five times as long as the upper arm, and the damping is light. The dimensionless relaxation times are equal to 0.1, which is much shorter than the natural periods of small oscillations for the undamped system; their natural circular frequencies are $\omega_1 = 1/\sqrt{1 + \lambda} = 0.91287$ and $\omega_2 = 1$ if Ω is zero. The external damping c_e may vary, while Ω is the main varying bifurcation parameter.

Firstly, the stationary solutions are investigated for the case $c_e = 0.02$, see Figure 2. The norm of the solution is defined as the Euclidean norm of the two-dimensional vector of angles $(q_2, q_3)^T$. The trivial solution loses its stability between $\Omega = \Omega_1 = 0.91398$ and $\Omega = \Omega_2 = 0.99878$, which are close to the two natural frequencies, in the same way as in a rotating shaft with unequal bending stiffness in two perpendicular directions. At Ω_1 , a branch of stable stationary solutions starts (SS in Figure 2), so this bifurcation is a supercritical pitchfork bifurcation. In these solutions, the angle q_2 is much larger in magnitude than q_3 and approaches $\pi/2$ for large values of Ω . At Ω_2 , a branch of unstable stationary

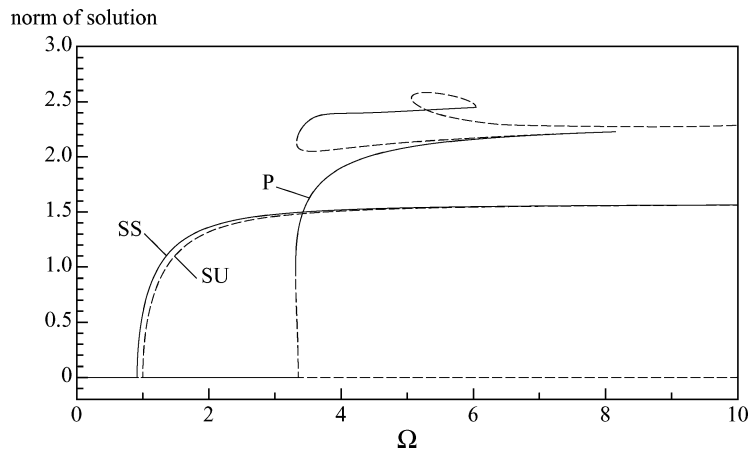


Figure 2. Response diagram for the double pendulum with varying spin rate Ω and parameter values $\lambda = 0.2$, $c_e = 0.02$, $c_2 = 0.01$, $k_2 = 0.1$, $c_3 = 0.01$, $k_3 = 0.1$. SS means stable stationary solutions; SU means unstable stationary solutions; P means periodic solutions. Full lines represent stable solutions and dashed lines denote unstable solutions.

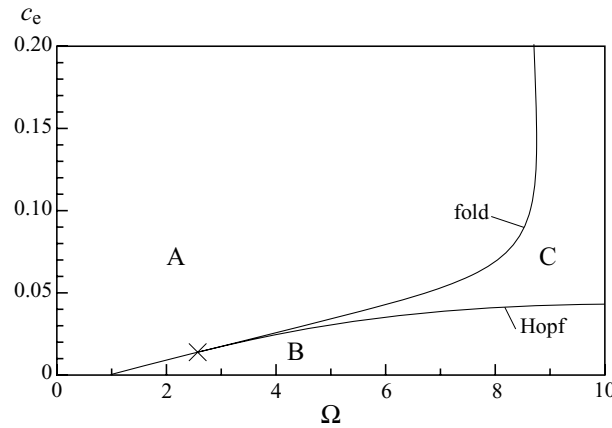


Figure 3. Partial bifurcation diagram when the spin rate Ω and the external damping coefficient c_e are varied. A branch of Hopf bifurcations for the trivial solution and a branch of fold bifurcations for periodic solutions is shown.

solutions starts (SU in Figure 2), so the bifurcation is a subcritical pitchfork bifurcation. In the solutions on this branch, q_3 is much larger in magnitude than q_2 and approaches $\pi/2$ for large values of Ω . No further bifurcations are found on these branches. The trivial solution loses its stability again at a Hopf bifurcation for $\Omega = \Omega_3 = 3.35346$. A second Hopf bifurcation occurs for $\Omega = \Omega_4 = 40.932$, after which the trivial solution becomes stable again. This last bifurcation is due to the Maxwell damping, which acts like a spring for high frequencies.

From the Hopf bifurcation at Ω_3 , a branch of unstable periodic solutions emerges for parameter values $\Omega < \Omega_3$, so the Hopf bifurcation is of the subcritical kind. If the branch is continued, fold or saddle-node bifurcations occur. In the first of these bifurcations, the periodic solutions become stable, in the second they become unstable again, in the third they become stable once again, but after the fourth fold bifurcation, the solutions remain unstable, although there is a fifth fold. The norm of the periodic solutions on this branch, which is defined as the Euclidean norm of the two-dimensional vector of maxima $(\max q_2, \max q_3)^T$, is also drawn in Figure 2.

For an example of the continuation of bifurcations in a two-parameter setting, the external damping coefficient c_e is chosen as a second variable parameter. Figure 3 shows a branch of Hopf bifurcations for the trivial solution and a branch of fold bifurcations for the resulting periodic solutions. The latter branch stops at the point of the branch with Hopf bifurcations where these bifurcations change from supercritical to subcritical at $\Omega = 2.5699$ and $c_e = 0.013904$. In a neighbourhood of this point, and in a neighbourhood of the trivial solution, there is a stable fixed point in the region A, an unstable fixed point circled by a stable limit cycle in region B, and a stable fixed point circled by an unstable limit cycle and a stable limit cycle in region C.

4. Motorcycle Dynamics

The second application concerns the dynamics of motorcycles. A survey of past research in this field can be found in [30–32]. The first study that included the major aspects contributing to the lateral stability of a motorcycle running straight ahead at a constant speed was made by Sharp [33]. This showed three basic ways in which the motion can become unstable: firstly, the capsizing instability like in an inverted pendulum; secondly, the wobble in which the front wheel behaves as a shimmying caster

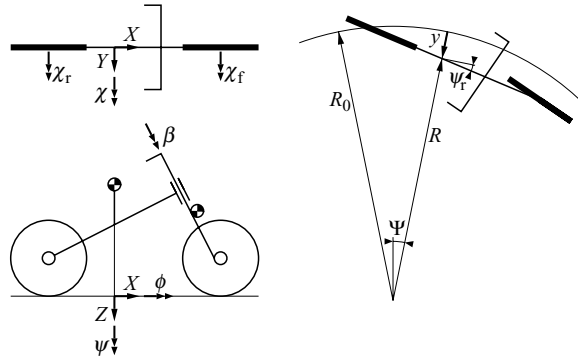


Figure 4. Generalized coordinates for the motorcycle model. On the left, the coordinates for running straight ahead and on the right, the alternative coordinates for cornering are shown.

wheel; and thirdly, the weave in which the complete motorcycle is involved with a combined rolling and yawing motion. A more detailed model, which could also be used for analysing the stability of the cornering motorcycle, was developed by Koenen [34]; this was still restricted to the linearized motion about a stationary trim condition. The model was developed further in [35], where simulations with the nonlinear model could be made.

The main purpose here is to show how the analysis procedure can be used to investigate this kind of systems. Therefore, a model with a limited number of degrees of freedom will be used that is an extension of the model in [33] to larger motions with the inclusion of a nonlinear tyre model. Essentially the same model was used in [36], but with a small difference in the tyre model. The mechanical model of the motorcycle consists of four rigid bodies: the rear frame with the rider rigidly attached to it, the front frame, and the two wheels. These bodies are interconnected by joints that allow one relative rotation, namely the steering head between the rear frame and the front frame and the wheel naves and axles. No suspension system is included in the model. Since no other constraints are introduced, the system has nine degrees of freedom: six for specifying the position and orientation of the rear frame and the three relative rotations at the joints. The reference system is rigidly connected to the road and is assumed to be an inertial system.

Two different cases will be considered: running on a level road in a straight line and negotiating a curve of constant radius. For each case, a different set of generalized coordinates will be employed to describe the configuration, see Figure 4. For the case of running on a straight road, the Cartesian coordinates and the modified Euler angles are adopted to describe the position of the origin of the rear frame assembly and its orientation. In the nominal upright position of the motorcycle, the origin is in the road surface directly below the centre of mass of the rear frame assembly. The translational degrees of freedom are denoted by X , Y , and Z , where X is the distance travelled along the road, Y is the lateral deviation to the right, and Z is the displacement toward the road surface. The Euler angles are the yaw angle ψ about the global Z -axis, the pitch angle χ about the intermediate lateral axis, and the roll angle ϕ about the longitudinal axis of the rear frame. Furthermore, the steering angle at the head is denoted by β and the relative rotations of the wheels are denoted by χ_r for the rear wheel and χ_f for the front wheel. The vector of generalized coordinates becomes $\mathbf{q}^T = (X, Y, Z, \psi, \chi, \phi, \beta, \chi_r, \chi_f)^T$. Of these, X , Y , ψ , χ_r , and χ_f are cyclic.

For the case of curving, the in-plane coordinates X and Y are replaced by polar coordinates with respect to the centre of curvature of the road, the angle Ψ , and the radius $R = R_0 - y$, where the radius is split into a nominal radius R_0 and a lateral deviation y . The yaw angle is similarly split into a

nominal yaw angle, the angle Ψ , and a relative yaw angle, ψ_r , as $\psi = \Psi + \psi_r$. The vector of generalized coordinates becomes $\mathbf{q}^T = (\Psi, y, Z, \psi_r, \chi, \phi, \beta, \chi_r, \chi_f)^T$, where Ψ , χ_r , and χ_f are cyclic. With these coordinates, a condition of stationary curving can be described by linearly increasing or decreasing angles Ψ , χ_r , and χ_f , while all other state variables are constant.

The dimensions and mechanical properties are essentially the same as those in [33] and are listed in the Appendix. The rear wheel is driven by the engine with a reduced engine constant K_m ; this means that the driving torque T_r on the rear wheel is given by

$$T_r = K_m(\dot{\chi}_r + V_0/R_e), \quad (8)$$

where V_0 is the velocity of the freely running motorcycle as determined by the throttle position and R_e is the nominal effective rolling radius of the rear wheel, so V_0/R_e is the nominal spin rate of the rear wheel. Note that $\dot{\chi}_r$ is negative for forward motion for the chosen generalized coordinates.

For cornering, a steering torque needs to be applied. The value of this torque is determined by a weak proportional-integral (PI) controller with the lateral deviation y as input, a proportional gain of 0.01 N, and an integrator gain of 0.01 N/s.

4.1. TYRE CONTACT KINEMATICS

The shape of the outer contour of the tyre is modelled by a surface of revolution, symmetric with respect to the equatorial plane, whose axis coincides with the axis of the wheel. The details of the tread profile are neglected. The shape is fully defined if a meridional section is given. A parametrization of the curve in this section, convenient for describing the contact between tyre and road, is by means of the angle γ that the tangent makes with the axis. The position of a point on the curve can then be described either directly with the distance from the equatorial plane, $\eta(\gamma)$, and the distance from the axis, $r(\gamma)$, or by a position on the evolute (the curve of centres of curvature [37]), given by the coordinates $c_\eta(\gamma)$ and $c_r(\gamma)$, and a radius of curvature, $\rho(\gamma)$, see Figure 5(a). The first way to describe the curve can be directly derived from the second way, while the inverse transformation involves differentiation. The option of describing the curve with the evolute is especially useful if the curve consists of a number of circular arcs that are connected without kinks, as shown in Figure 5(b): the evolute reduces to a series of points, with a discontinuous jump at the transition points. In the example here only the case of a toroidal shape is used, where the evolute is just a point.

A generic wheel is denoted by the letter 'w', which can denote either the rear wheel or the front wheel. The absolute position vector of the centre of the wheel (the point of intersection of the axis of the

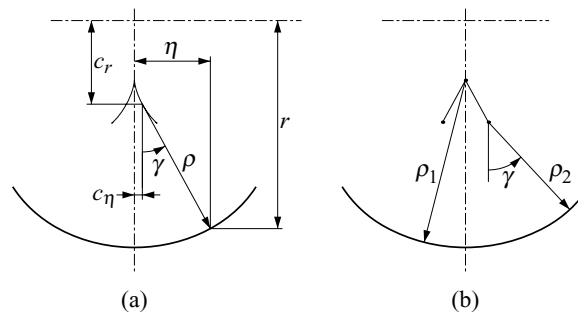


Figure 5. Shape of the tyre tread.

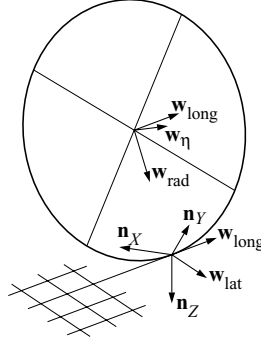


Figure 6. Unit vectors associated with the wheel. Note that the inclination angle γ_w is negative for the displayed configuration.

wheel and the equatorial plane) is denoted by \mathbf{w}_0 . Several unit vectors can be associated with the wheel, as shown in Figure 6. Firstly, $(\mathbf{n}_X, \mathbf{n}_Y, \mathbf{n}_Z)$ is a system of unit vectors in the global coordinate directions. The orthogonal body-fixed unit vectors attached to the centre of the wheel are $(\mathbf{w}_\xi, \mathbf{w}_\eta, \mathbf{w}_\zeta)$, where \mathbf{w}_η points in the direction of the wheel axis. As the absolute value of the rotation of a symmetric wheel about its axis is unimportant, it is convenient to have a rotated system of unit vectors $(\mathbf{w}_{\text{long}}, \mathbf{w}_\eta, \mathbf{w}_{\text{rad}})$, where \mathbf{w}_{long} is parallel to the ground surface and points in the forward direction and \mathbf{w}_{rad} points radially in the downward direction. In the ground surface a unit vector \mathbf{w}_{lat} is defined such that $(\mathbf{w}_{\text{long}}, \mathbf{w}_{\text{lat}}, \mathbf{n}_Z)$ forms a right-handed orthogonal system. If the unit vectors \mathbf{n}_Z and \mathbf{w}_η are given, the inclination angle γ_w ($-\pi/2 < \gamma_w < \pi/2$) can be calculated from $\gamma_w = \arcsin(\mathbf{w}_\eta \cdot \mathbf{n}_Z)$, while $\cos \gamma_w = \sqrt{1 - \sin^2 \gamma_w}$. Then, the other unit vectors can be calculated as

$$\mathbf{w}_{\text{long}} = \frac{\mathbf{w}_\eta \times \mathbf{n}_Z}{|\mathbf{w}_\eta \times \mathbf{n}_Z|} = \frac{\mathbf{w}_\eta \times \mathbf{n}_Z}{\cos \gamma_w}, \quad (9)$$

$$\mathbf{w}_{\text{rad}} = \mathbf{w}_{\text{long}} \times \mathbf{w}_\eta = \frac{\mathbf{n}_Z - \mathbf{w}_\eta \sin \gamma_w}{\cos \gamma_w}, \quad (10)$$

$$\mathbf{w}_{\text{lat}} = \mathbf{n}_Z \times \mathbf{w}_{\text{long}} = \frac{\mathbf{w}_\eta - \mathbf{n}_Z \sin \gamma_w}{\cos \gamma_w}. \quad (11)$$

The standard contact point, as it is defined in the SAE recommended practice [38], is the intersection point of the radial vector \mathbf{w}_{rad} with the ground. For motorcycles, this point can be outside the contact patch if the inclination angle is large; it is more convenient to define a contact point that is approximately in the centre of the contact patch. The nominal undeflected contact point, as it is defined here, is the point which would have the deepest penetration into the road surface (or, alternatively, the smallest distance to the road surface) if the tyre were rigid and the road deformable. The position of this point can be found as

$$\mathbf{w}_{\text{cu}} = \mathbf{w}_0 + c_\eta(\gamma_w)\mathbf{w}_\eta + c_r(\gamma_w)\mathbf{w}_{\text{rad}} + \rho(\gamma_w)\mathbf{n}_Z \quad (12)$$

if a description with an evolute is chosen, or as

$$\mathbf{w}_{\text{cu}} = \mathbf{w}_0 + \eta(\gamma_w)\mathbf{w}_\eta + r(\gamma_w)\mathbf{w}_{\text{rad}} \quad (13)$$

if a direct description is used. The nominal deflected contact point is defined as the intersection point of the vertical line through the undeformed contact point with the road surface. The deflection of the

tyre in the normal direction, ϵ_n , is therefore

$$\epsilon_n = \mathbf{w}_{cu} \cdot \mathbf{n}_Z \quad (14)$$

and the position vector \mathbf{w}_{cd} of the nominal deflected contact point is given by

$$\mathbf{w}_{cd} = \mathbf{w}_{cu} - \epsilon_n \mathbf{n}_Z. \quad (15)$$

Three slip velocities at the contact point are discerned: the longitudinal slip velocity, the lateral slip velocity, and the normal spin rate. Because of deformations in the tyre material, the slip velocities differ from the values that would be valid for a rigid tyre. This effect can be partly taken into account by introducing effective rolling radii. This is included here by considering the lateral and longitudinal velocities of points between the nominal undeformed and the nominal deformed contact points. The longitudinal slip is defined as

$$\dot{\epsilon}_{long} = \{\dot{\mathbf{w}}_0 + \boldsymbol{\omega}_0 \times [\mathbf{w}_{cu} - (1 - \xi_{long})\epsilon_n \mathbf{n}_Z - \mathbf{w}_0]\} \cdot \mathbf{w}_{long}, \quad (16)$$

where $\boldsymbol{\omega}_0$ is the absolute angular velocity of the wheel. The lateral slip is defined as

$$\dot{\epsilon}_{lat} = \{\dot{\mathbf{w}}_0 + \boldsymbol{\omega}_0 \times [\mathbf{w}_{cu} - (1 - \xi_{lat})\epsilon_n \mathbf{n}_Z - \mathbf{w}_0]\} \cdot \mathbf{w}_{lat}. \quad (17)$$

The coefficients ξ_{long} and ξ_{lat} are numerical coefficients, usually between zero and one. The normal spin rate is simply the component of the angular velocity in the direction of the normal vector,

$$\omega_n = -\boldsymbol{\omega}_0 \cdot \mathbf{n}_Z. \quad (18)$$

The dimensionless, or reduced, slip quantities are obtained by dividing the slip velocities by the reference velocity V_w of the wheel. Normally, this velocity is defined as the speed with which the undeformed tyre surface moves through the contact patch. For simplicity, this is taken here as the component of the velocity of the centre of the wheel in the longitudinal direction,

$$V_w = \dot{\mathbf{w}}_0 \cdot \mathbf{w}_{long}. \quad (19)$$

With this and the nominal wheel radius R_w , the dimensionless slip quantities become

$$s_{long} = \dot{\epsilon}_{long}/V_w, \quad s_{lat} = \dot{\epsilon}_{lat}/V_w, \quad s_n = \omega_n R_w/V_w. \quad (20)$$

4.2. TYRE FORCES

The tyre forces are given by the constitutive relations. We propose here relatively simple expressions for the tyre forces that use just a few parameters. This model captures the behaviour at small slips, where it reduces to a linear model, and at very high slips, where it approaches the Coulomb friction law. In between, the description is not as accurate as more advanced models given, for instance, in [39]. The parameters needed are the coefficients of a linearized model, the coefficient of friction, and also the tyre normal stiffness and damping.

The tyre forces are the resultant forces and moments of stresses that the road exerts on the tyre. The components are chosen as the algebraic duals of the normal deflection, the slip velocities, and the normal spin rate. The normal force F_n acts in the direction of the normal of the road, the longitudinal force F_{long} in the direction opposite to \mathbf{w}_{long} , the lateral force F_{lat} in the direction opposite to \mathbf{w}_{lat} , and the normal moment M_n in the direction opposite to the normal to the road surface. Additional components of the moment may arise if the resultant normal force has a line of action that is some distance from the nominal contact point; these components will be neglected. The contribution of the tyre forces and moment to the virtual power is

$$\delta P = -F_n \delta \epsilon_n - F_{\text{long}} \delta \dot{\epsilon}_{\text{long}} - F_{\text{lat}} \delta \dot{\epsilon}_{\text{lat}} - M_n \delta \omega_n. \quad (21)$$

The prefixed δ denotes a virtual variation. Note that the line of action of the longitudinal as well as of the lateral force is below the road surface because of the coefficients ξ_{long} and ξ_{lat} in the definitions of the longitudinal and lateral slip velocities in Equations (16) and (17).

The normal force is assumed to be a linear combination of the normal deflection and its rate. Since the normal force cannot be negative when the wheel loses contact with the ground, the normal deflection is smoothed as

$$\tilde{\epsilon}_n = \frac{1}{2} \epsilon_{n0} \left[\frac{\epsilon_n}{\epsilon_{n0}} + \sqrt{\left(\frac{\epsilon_n}{\epsilon_{n0}} \right)^4 + 1} \right] > 0. \quad (22)$$

The normal force is then given by

$$F_n = K_n \tilde{\epsilon}_n + C_n \dot{\tilde{\epsilon}}_n, \quad (23)$$

where K_n is the spring constant and C_n is the damping constant.

An auxiliary slip quantity, s_{tot} , called the total slip, is defined as

$$s_{\text{tot}} = \sqrt{s_{\text{long}}^2 + s_{\text{lat}}^2}. \quad (24)$$

The equations for the steady-state values of the tyre forces are

$$F_{\text{long,ss}} = \frac{C_1 F_n s_{\text{long}}}{\sqrt{1 + B^2 s_{\text{tot}}^2}}, \quad (25)$$

$$F_{\text{lat,ss}} = \frac{C_1 F_n (s_{\text{lat}} - \xi_{\text{eq}} s_n / \sqrt{1 + B^2 s_{\text{tot}}^2})}{\sqrt{1 + B^2 s_{\text{tot}}^2}}, \quad (26)$$

$$M_{n,ss} = \frac{\xi_{\text{eq}} R_w C_1 F_n s_{\text{lat}}}{1 + B^2 s_{\text{tot}}^2}, \quad (27)$$

where C_1 is the ratio of the cornering stiffness and the normal force, the coefficient ξ_{eq} is equal to the ratio of the cornering stiffness and the camber stiffness, $B = C_1 / \mu_w$, and μ_w is the coefficient of friction for large sliding speeds. These expressions always give a nonnegative dissipation, but they cannot be derived from a Rayleigh dissipation function. For zero longitudinal slip and with the tyre parameters given in the Appendix, the lateral force and the aligning moment for several inclination angles are shown in Figure 7. The normal spin is calculated from the inclination angle as $s_n = R_w \sin \gamma_w / (c_r + \rho \cos \gamma_w)$.

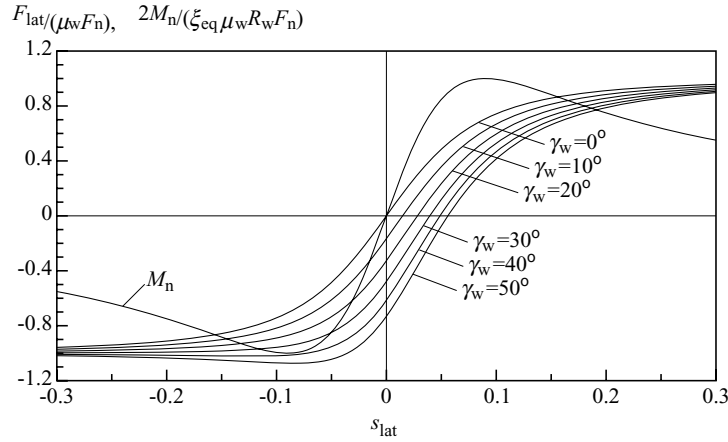


Figure 7. Tyre characteristics for zero longitudinal slip. The steady-state dimensionless aligning moment and lateral force are shown for the inclination angles $\gamma_w = 0, 10, 20, 30, 40,$ and 50° . Note that the aligning moment does not depend on γ_w .

Note that for opposite signs of the slip and the inclination angle, the lateral force can be larger than the friction coefficient for large slips multiplied by the normal force. These curves may be compared with the tyre characteristics shown in [39, p. 524]: the broad tendency for the lateral force is comparable, while the aligning moments are larger in the present model.

For nonstationary behaviour, the tyre forces are related to their steady-state values through first-order filters as

$$\dot{F}_{\text{long}} = \frac{V_w}{\sigma_{\text{long}}} (F_{\text{long,ss}} - F_{\text{long}}), \quad (28)$$

$$\dot{F}_{\text{lat}} = \frac{V_w}{\sigma_{\text{lat}}} (F_{\text{lat,ss}} - F_{\text{lat}}), \quad (29)$$

$$\dot{M}_n = \frac{V_w}{\sigma_n} (M_{n,ss} - M_n), \quad (30)$$

where σ_{long} , σ_{lat} , and σ_n are relaxation lengths that depend linearly on the modified normal deflection $\tilde{\xi}_n$ as

$$\sigma_{\text{long}} = \sigma_{\text{long},0} + \sigma_{\text{long},1} \tilde{\xi}_n, \quad (31)$$

and similarly for the other relaxation lengths.

4.3. RESULTS

Firstly, the case in which the motorcycle is nominally running straight ahead on a level road with a constant speed is investigated. The main varying parameter is V_0 , the velocity of the freely running motorcycle, while default values for the other parameters are listed in the Appendix. In the present context of human control, a stationary solution is called, rather arbitrarily, mildly unstable if the unstable eigenvalues have absolute values that are smaller than 2 s^{-1} , in which case it is fairly easy to stabilize these motions. On the other hand, a solution will be called strongly unstable if the absolute value of an unstable eigenvalue is larger than 4 s^{-1} , in which case it is hard to stabilize the motion.

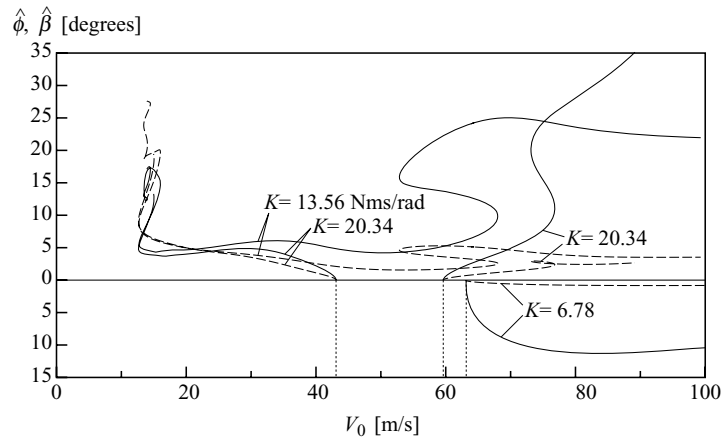


Figure 8. The amplitude of the steering angle $\hat{\beta}$ (full lines) and the roll angle $\hat{\phi}$ (dashed lines) for periodic solutions for three values of the steering head damping coefficient K . The amplitudes for the wobble motion are drawn in the downward direction, while the amplitudes for the weave motion are drawn in the upward direction.

For the default parameter values and without rider control, the nominal solution appears to be unstable for all forward velocities. From a low velocity of $V_0 \approx 2.5$ m/s, up to a Hopf bifurcation point at $V_0 = 63.16$ m/s, the instability is only mild, and above $V_0 \approx 5$ m/s, this corresponds to a capsizing mode; the instability is as in an inverted pendulum. The velocity interval of stable motions found in [33] can be attributed to a difference in the model for the contact between tyre and road. At the Hopf bifurcation, a supercritical branch of periodic solutions emerges, that is, the branch bends to the direction in which the pair of critical eigenvalues has positive real parts. The motion on this branch can be described as a wobble, where the front wheel behaves as a shimmying caster wheel. Along this branch, the capsizing instability disappears at $V_0 = 66.96$ m/s. The amplitude of the roll angle and the steering angle are shown in the lower part of Figure 8. The frequency of this wobble motion is about 10 Hz and varies only little with the nominal velocity.

The wobble instability can be suppressed by increasing the steering head damping. For instance, if the damping coefficient is increased by a factor two, from $K = 6.78$ Nms/rad to $K = 13.56$ Nms/rad, the wobble instability is suppressed up to $V_0 = 100$ m/s. However, the weave mode, in which the yaw, roll, as well as the steering angle participate significantly, becomes less damped. This is another example of a destabilizing effect of the internal damping, as in the example of the rotating double pendulum. If the damping coefficient is further increased to $K = 20.34$ Nms/rad, two Hopf bifurcations are found at $V_0 = 43.09$ m/s and $V_0 = 59.62$ m/s; between these values the nominal motion is unstable. The emerging branches of periodic motions, as shown in the upper part of Figure 8, are of the subcritical kind and these motions are strongly unstable. Even for $K = 13.56$ Nms/rad, a disconnected branch of unstable limit cycles is found, which is also shown in Figure 8. The end of the branches are just the points where the calculations are stopped or the numerical procedure failed to converge and have no special meaning. The presence of this branch of unstable periodic motions means that for small perturbations of the nominal solution, the motion remains mildly unstable, but if the initial perturbations are of the same order of magnitude as the amplitude of the unstable limit cycle, the amplitude may strongly increase to a catastrophic extent. An initial steer angle of 5° and an initial roll angle of 2° can be sufficient for this to happen.

The influence of changing other parameters can be investigated in the same way. For instance, if the height of the centre of gravity is halved from 0.615696 to 0.307848 m, the capsizing mode becomes stable between $V_0 = 5.30$ and $V_0 = 15.90$ m/s, and increases the velocity for the wobble instability to

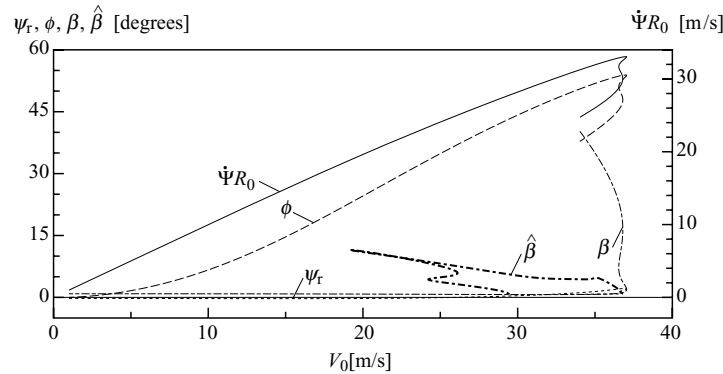


Figure 9. Response diagram for negotiating a curve with a radius of 100 m. The stationary values for the trajectory speed Ψ_{R_0} (full line), the relative yaw angle ψ_r (dotted line), the roll angle ϕ (dashed line), and the steering angle β (dashed-dotted line) are shown. The maximal values for the steering angle $\hat{\beta}$ for the cornering wobble motion are drawn with thick dashed-dotted line.

$V_0 = 69.85$ m/s; a reduction of the lateral tyre stiffness with 20% increases the velocity of the wobble instability to $V_0 = 68.27$ m/s.

Next, the behaviour during the negotiation of a curve of constant radius of $R_0 = 100$ m is investigated. Figure 9 shows the relative yaw, roll, and steering angles for stationary cornering, depending on the parameter V_0 as appears in Equation (8). This is only equal to the speed along the curve, Ψ_{R_0} , for low velocities, as can be seen from the figure. With increasing speed, the roll angle increases initially quadratically, while the relative yaw angle and steering angle remain small and close to their initial values which are determined by the kinematics. At $V_0 = 26.55$ m/s, a Hopf bifurcation occurs, which can be characterized as a cornering wobble motion with a frequency of about 7 Hz. Further along the branch of stationary solutions, a fold or limit point is encountered with $V_0 = 37.05$ m/s. After this point, the solution is strongly unstable and the speed along the curve decreases. The maximum speed is limited by the saturation of the friction between tyre and road. For the front tyre, the friction saturates and the lateral slip becomes large, while the lateral slip for the rear tyre remains moderate. The branch of periodic solutions that starts at the Hopf bifurcation has been calculated; only the maximal steering angle, $\hat{\beta}$, is shown in Figure 9. The bifurcation appears to be subcritical, and at $V_0 = 24$ m/s, the front wheel loses contact with the ground during a part of the periodic motion. This jumping is due to the absence of a suspension system in the model. The branch ends at another Hopf bifurcation that is close to the limit point.

Although the behaviour up to about 25 m/s is hardly affected by small variations in the modelling of tyre forces, the ultimate behaviour of the solutions is sensitive to changes. As an example, the behaviour for the case in which the friction coefficient of the front wheel is increased by 5% is investigated, see Figure 10. Nearly up to the limit point, the change in the behaviour is small, but then, instead of turning back, the branch can be continued for a further increase of V_0 . The velocity along the curve decreases, however, and the steering angle becomes negative, while the relative yaw angle becomes large; this part of the motion is strongly unstable. For the rear tyre, the friction saturates and the lateral slip becomes large, while the lateral slip for the front tyre remains moderate. The branch of wobbling motions now emerges at a Hopf bifurcation at $V_0 = 26.64$ m/s, but it does not end at a second Hopf bifurcation. Instead, it ends in a homoclinic bifurcation, where the periodic motion comes close to the unstable stationary solution, while the period increases without bound. Whereas the behaviour in the previous case can be classified as about neutral steer, the present case resembles oversteer behaviour. If the results for cornering are compared with the results obtained in [36], it is seen that the ultimate results near

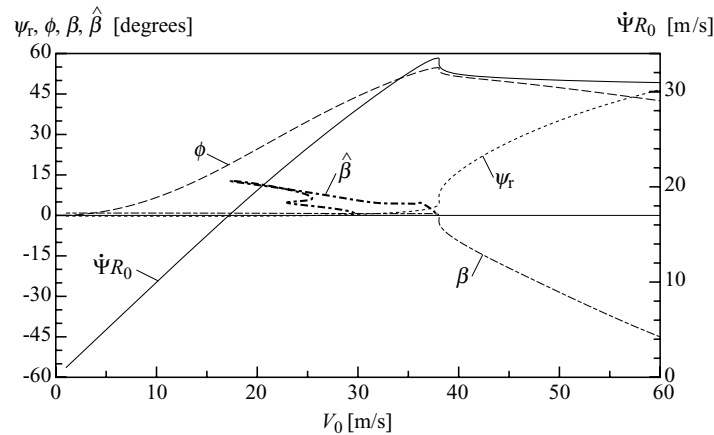


Figure 10. Response diagram for negotiating a curve as in Figure 9, but with $\mu_r = 1.05$.

saturation of the friction differ considerably, so they depend in a sensitive way on the uncertain details of the tyre force models in this range of slips.

5. Conclusions

It has been shown how a multibody dynamics program and a continuation program can be used to investigate the nonlinear behaviour of mechanical systems. It is possible to calculate branches of stationary and periodic solutions under the variation of a parameter and to determine their stability and bifurcations. The calculation of branches of unstable solutions cannot be done so easily by other means.

Despite these successes, there are some limitations in the methods of the programs that are used. The generation of the equations of motion in a symbolic form has the advantage that the equations are available for further processing, so derivatives can be obtained fairly easily. Disadvantages of symbolic programs are that the resulting equations tend to increase quickly in extent with an increasing problem size and it is not straightforward to deal with systems with kinematic closed loops, where the bodies are interconnected in such a way as to form circuits. The continuation software used has the limitations that it cannot take into account symmetries which are present in the system, that the equations have to be smooth, so discontinuities have to be approximated by smooth functions, and that some elementary local bifurcations cannot be continued in a two-parameter setting. The method used for discretizing periodic solutions can be less efficient and less flexible than alternative methods.

The application to the dynamics of a motorcycle, nevertheless, has shown that the proposed procedure can be used for practical engineering problems. It is planned to direct future works in this application toward extending the model to include the suspension system and control input by the rider.

Appendix: Motorcycle Data

In this appendix, the default parameter values of the motorcycle model in Section 4 are listed. Most of these values are taken from [33], with some additional parameters for the tyre model and the mass distribution. Figure 11 gives the main dimensions, while the symbols for the parameters with their values and a description are listed in Tables 1 and 2. Note that the effective rolling radius R_e in Equation (8) can

Table 1. Motorcycle data (Latin symbols).

Symbol	Value	Description
a	0.9485 m	Distance to steering head
b	0.4798 m	Distance to the rear wheel contact point
$C_{1,f}$	11.096	Front tyre cornering stiffness coefficient
$C_{1,r}$	11.096	Rear tyre cornering stiffness coefficient
$C_{n,f}$	500 Ns/m	Front tyre normal damping coefficient
$C_{n,r}$	500 Ns/m	Rear tyre normal damping coefficient
$c_{r,f}$	0.2448 m	Front tyre radius to the torus centre
$c_{r,r}$	0.2448 m	Rear tyre radius to the torus centre
$C_{xz,f}$	0 kgm ²	Front frame assembly product of inertia
$C_{xz,r}$	1.7354 kgm ²	Rear frame assembly product of inertia
e	0.024384 m	Coordinate of centre of mass of front frame assembly
f	0.0283464 m	Coordinate of centre of mass of rear frame assembly
h	0.615696 m	Height of centre of mass of rear frame assembly
$I_{x,f}$	1.2338 kgm ²	Front frame assembly longitudinal moment of inertia
$I_{x,r}$	31.1838 kgm ²	Rear frame assembly longitudinal moment of inertia
$i_{y,f}$	0.7186 kgm ²	Front wheel axial moment of inertia
$i_{y,r}$	1.0508 kgm ²	Rear wheel reduced axial moment of inertia
$I_{y,f}$	1.6 kgm ²	Front frame assembly transverse moment of inertia
$I_{y,r}$	42.0 kgm ²	Rear frame assembly transverse moment of inertia
$I_{z,f}$	0.442 kgm ²	Front frame assembly vertical moment of inertia
$I_{z,r}$	21.0694 kgm ²	Rear frame assembly vertical moment of inertia
K	6.78 Nms/rad	Steering head damping constant
K_m	10.0 Nms/rad	Reduced engine constant
$K_{n,f}$	100672.0 N/m	Front tyre normal stiffness
$K_{n,r}$	142627.0 N/m	Rear tyre normal stiffness
l	0.9347 m	Distance to the front tyre contact point
M_f	30.6472 kg	Front frame assembly mass
M_r	217.449 kg	Rear frame assembly mass
R_f	0.3048 m	Deformed front tyre radius
R_r	0.3048 m	Deformed rear tyre radius

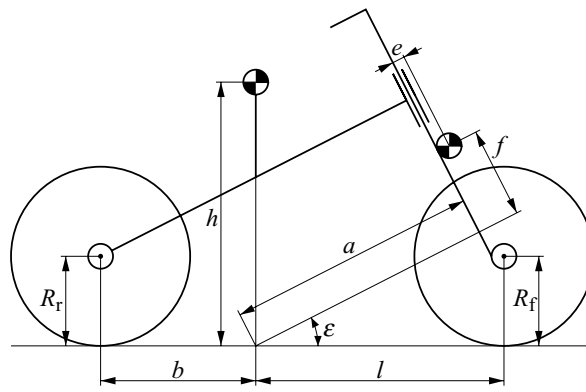


Figure 11. Main dimensions for the motorcycle.

Table 2. Motorcycle data (Greek symbols).

Symbol	Value	Description
ε	0.4715 rad	Steering head inclination angle
$\epsilon_{n0,f}$	0.0005 m	Front tyre normalization parameter for the normal force
$\epsilon_{n0,r}$	0.0005 m	Rear tyre normalization parameter for the normal force
$\xi_{eq,f}$	0.084	Front tyre parameter for the lateral force
$\xi_{eq,r}$	0.084	Rear tyre parameter for the lateral force
$\xi_{lat,f}$	0.2	Front tyre parameter for the lateral slip
$\xi_{lat,r}$	0.2	Rear tyre parameter for the lateral slip
$\xi_{long,f}$	0.33	Front tyre parameter for the longitudinal slip
$\xi_{long,r}$	0.33	Rear tyre parameter for the longitudinal slip
μ_f	1.0	Front tyre coefficient of friction
μ_r	1.0	Rear tyre coefficient of friction
ρ_f	0.07 m	Radius of toroidal part of front tyre
ρ_r	0.07 m	Radius of toroidal part of rear tyre
$\sigma_{lat,0,f}$	0.04 m	Front tyre lateral force relaxation length parameter
$\sigma_{lat,0,r}$	0.04 m	Rear tyre lateral force relaxation length parameter
$\sigma_{lat,1,f}$	20.0	Front tyre lateral force relaxation length parameter
$\sigma_{lat,1,r}$	20.0	Rear tyre lateral force relaxation length parameter
$\sigma_{long,0,f}$	0.04 m	Front tyre longitudinal force relaxation length parameter
$\sigma_{long,0,r}$	0.04 m	Rear tyre longitudinal force relaxation length parameter
$\sigma_{long,1,f}$	20.0	Front tyre longitudinal force relaxation length parameter
$\sigma_{long,1,r}$	20.0	Rear tyre longitudinal force relaxation length parameter
$\sigma_{n,0,f}$	0.02 m	Front tyre aligning moment relaxation length parameter
$\sigma_{n,0,r}$	0.02 m	Rear tyre aligning moment relaxation length parameter
$\sigma_{n,1,f}$	10.0	Front tyre aligning moment relaxation length parameter
$\sigma_{n,1,r}$	10.0	Rear tyre aligning moment relaxation length parameter

be calculated from the deformed radius, the nominal load distribution between the wheels, the normal stiffness, and the longitudinal slip parameter ξ_{long} .

Acknowledgement

This work was supported by a research grant from the Engineering and Physical Sciences Research Council (EPSRC) of the U.K.

References

1. Schiehlen, W. (ed.), *Multibody Systems Handbook*, Springer-Verlag, Berlin, 1990.
2. Kortüm, W. and Sharp, R. S. (eds.), *Multibody Computer Codes in Vehicle System Dynamics*, Vehicle System Dynamics, Vol. 22(Suppl.), Swets and Zeitlinger, Lisse, The Netherlands, 1993.
3. Schiehlen, W., 'Multibody system dynamics, roots and perspectives', *Multibody System Dynamics* **1**, 1997, 149–188.

4. Shabana, A. A., 'Flexible multibody dynamics, review of past and recent developments', *Multibody System Dynamics* **1**, 1997, 189–222.
5. Allgower, E. L. and Georg, K., 'Numerical path following', in *Handbook of Numerical Analysis, Vol. V: Techniques of Scientific Computing (Part 2)*, P. G. Ciarlet and J. L. Lions (eds.), Elsevier, Amsterdam, 1997, pp. 3–207.
6. Guckenheimer, J. and Holmes, P., *Nonlinear Oscillations, Dynamical Systems, and Bifurcations of Vector Fields*, Springer-Verlag, New York, 1983.
7. Thompson, J. M. T. and Stewart, H. B., *Nonlinear Dynamics and Chaos, Geometrical Methods for Engineers and Scientists*, Wiley, Chichester, UK, 1986. [2nd edn., 2002]
8. Kuznetsov, Y. A., *Elements of Applied Bifurcation Theory*, 2nd edn., Springer-Verlag, New York, 1998. [1st edn., 1995]
9. Roth, B. and Freudenstein, F., 'Synthesis of path-generating mechanisms by numerical methods', *ASME Journal of Engineering for Industry* **85**, 1963, 298–306.
10. Wampler, C. W., Morgan, A. P., and Sommese, A. J., 'Numerical continuation methods for solving polynomial systems arising in kinematics', *ASME Journal of Mechanical Design* **112**, 1990, 59–68.
11. Crisfield, M. A., *Non-Linear Finite Element Analysis of Solids and Structures, Vol. 1: Essentials*, Wiley, Chichester, UK, 1991.
12. Wriggers, P. and Simo, J. C., 'A general procedure for the direct computation of turning and bifurcation points', *International Journal for Numerical Methods in Engineering* **30**, 1990, 155–176.
13. Cardona, A. and Huespe, A., 'Continuation methods for tracing the equilibrium path in flexible mechanism analysis', *Engineering Computations* **15**, 1998, 190–220.
14. Meijaard, J. P., 'Direct determination of periodic solutions of the dynamical equations of flexible mechanisms and manipulators', *International Journal for Numerical Methods in Engineering* **32**, 1991, 1691–1710.
15. Meijaard, J. P., 'Direct determination of periodic solutions of mechanical dynamical systems', *Archive of Applied Mechanics* **64**, 1994, 249–257.
16. Sayers, M. W., 'Symbolic Computer Methods to Automatically Formulate Vehicle Simulation Codes', Doctoral Dissertation, The University of Michigan, Ann Arbor, MI, 1990.
17. Sayers, M. W., 'Symbolic computer language for multibody systems', *Journal of Guidance, Control, and Dynamics* **14**, 1991, 1153–1163.
18. Sayers, M. W., 'Symbolic vector/dyadic multibody formalism for tree-topology systems', *Journal of Guidance, Control, and Dynamics* **14**, 1991, 1240–1250.
19. Anon., *AutoSimTM Reference Manual Version 2.5+*, Mechanical Simulation Corporation, Ann Arbor, MI, 1997.
20. Kane, T. R., *Dynamics*, Holt, Rinehart and Winston, New York, 1968.
21. Steele, G. L. Jr., *Common Lisp, the Language*, 2nd edn., Digital Press, USA, 1990.
22. Doedel, E., Keller, H. B., and Kernevez, J. P., 'Numerical analysis and control of bifurcation problems, (I) bifurcation in finite dimensions', *International Journal of Bifurcation and Chaos* **1**, 1991, 493–520.
23. Doedel, E., Keller, H. B., and Kernevez, J. P., 'Numerical analysis and control of bifurcation problems, (II) bifurcation in infinite dimensions', *International Journal of Bifurcation and Chaos* **1**, 1991, 745–772.
24. Doedel, E., Champneys, A. R., Fairgrieve, T. F., Kuznetsov, Y. A., Sandstede, B., and Wang, X. J., 'AUTO 97: Continuation and bifurcation software for ordinary differential equations', Technical Report, Department of Computer Science, Concordia University, Montreal, 1997.
25. Kane, T. R. and Levinson, D. A., 'A multibody motion stability analysis', *Multibody System Dynamics* **3**, 1999, 287–299.
26. Sharp, R. S., 'The parametrically excited multi-pendulum', *Multibody System Dynamics* **5**, 2001, 303–313, erratum, *ibid.* **6**, 2001, 301–302.
27. Graham, D. and McRuer, D., 'Retrospective essay on nonlinearities in aircraft flight control', *Journal of Guidance, Control, and Dynamics* **14**, 1991, 1089–1099.
28. Gantmacher, F., *Lectures in Analytical Mechanics*, Mir, Moscow, 1970.
29. Meijaard, J. P., 'Numerical continuation methods and bifurcation analysis applied to multibody system dynamics', in *Proceedings of the ASME 2003 Design Engineering Technical Conferences and Computers and Information in Engineering Conference*, A. A. Shabana (ed.), The American Society of Mechanical Engineers, New York, 2003, paper DETC2003/VIB-48310, Vol. 5A, pp. 63–70.
30. Sharp, R. S., 'A review of motorcycle steering behaviour and straight line stability characteristics', in *Motorcycle Dynamics and Rider Control*, SP-428, Society of Automotive Engineers, Warrendale, PA, 1978, paper 780303, pp. 1–6.
31. Sharp, R. S., 'The lateral dynamics of motorcycles and bicycles', *Vehicle System Dynamics* **14**, 1985, 265–283.
32. Sharp, R. S., 'Stability, control, and steering responses of motorcycles', *Vehicle System Dynamics* **35**, 2001, 291–318.
33. Sharp, R. S., 'The stability and control of motorcycles', *Journal of Mechanical Engineering Science* **13**, 1971, 316–329.
34. Koenen, C., 'The Dynamic Behaviour of a Motorcycle When Running Straight Ahead and When Cornering', Doctoral Dissertation, Delft University Press, Delft, The Netherlands, 1983.
35. Sharp, R. S. and Limebeer, D. J. N., 'A motorcycle model for stability and control analysis', *Multibody System Dynamics* **6**, 2001, 123–142.

36. Meijaard, J. P. and Popov, A. A., 'Application of non-linear dynamics to instability phenomena in motorcycles' [The Dynamics of Vehicles on Roads and on Tracks, M. Abe (ed.), Proceedings of the 18th IAVSD Symposium, Kanagawa, Japan, August 24–30, 2003], *Vehicle System Dynamics* **41**(Suppl.), 2004, 567–576.
37. Struik, D. J., *Lectures on Classical Differential Geometry*, Addison-Wesley, Cambridge, MA, 1950.
38. Anon., *Vehicle Dynamics Terminology, SAE J670e*, Society of Automotive Engineers, Warrendale, PA, 1978.
39. Pacejka, H. B., *Tyre and Vehicle Dynamics*, Butterworth-Heinemann, Oxford, 2002.